Fast-Track Computational Access to Reaction Mechanisms Provides Comprehensive Insights into Aminolysis Postpolymerization Modification Reactions

Kiho Matsubara[a], Li-Chieh Chou[a], Hideki Amii[a], and Ryohei Kakuchi[a]*

[a.] Division of Molecular Science, Faculty of Science and Technology, Gunma University, 1-5-1 Tenjin, Kiryu, Gunma 376-8515, Japan

(TOC graphic)

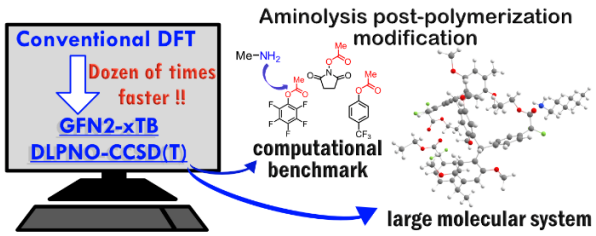

for Table of Contents use only

ABSTRACT: With the aim of providing a computational guideline for activated ester–amine chemistry, a series of activated esters commonly used in polymer synthesis have been systematically analyzed at the DLPNO-CCSD(T) level of theory by taking advantage of the recently developed density functional theory-based semiempirical method GFN2-xTB. The fast-track computational analysis based on the GFN2-xTB and DLPNO-CCSD(T) methods can explain well the experimentally observed reactivity in aminolysis postpolymerization modification reactions. Moreover, transition state search calculations can be performed with realistic model structures consisting of more than a hundred atoms, offering a new approach for reaction profiling for large molecular systems without further approximations. The realistic reaction profiling allows a preliminary assessment and visualization of the polymer effect during the postpolymerization modification at the DLPNO-CCSD(T) level of theory. This study offers a computational compass for activated ester–amine chemistry for application in postpolymerization modification reactions.

Introduction

With the integration of efficient organic transformation reactions such as the so-called click reactions, —which include Cu-catalyzed azide–alkyne cycloaddition[1-4], thiol-e(y)ne,[5] Diels–Alder,[6] epoxide nucleophiles,[7] and activated ester–amine chemistries,[8] in modern polymer chemistry[9-11]—postpolymerization modification processes have emerged as a useful synthetic tool toward functionalized polymeric materials. In particular, the synthetic utility of the activated ester–amine chemistry deserves special mention due to its operational simplicity and the commercial availability of functional amines. In this context, a number of activated esters have

been incorporated in polymer synthesis, including *N*-hydroxysuccinimide,[12] pentafluorophenyl,[13-16] 4-nitrophenyl,[17] hexafluoroisopropyl,[18] and 4-dialkylsulfonium phenyl esters,[19] providing access to functional polymer materials via simple aminolysis reactions. As the number of available activated esters in polymer science increases, a theoretical guidance for activated ester chemistry would be highly desirable for the development of material applications. In particular, the computational analysis of activated esters could facilitate the understanding of postpolymerization modification reactions, which exhibit inherent difficulties compared with standard organic chemistry. For instance, in postpolymerization modification reactions, polymer solubility is frequently a decisive factor that can interfere in gaining experimental insight into reaction profiling.

Recently, our group proposed the postpolymerization modification reactions based on the aminolysis of α,α-difluoroacetate esters.[20-22] In those studies, we rationalized the experimental conditions for the aminolysis postpolymerization modifications on the basis of mechanistic information obtained by means of density functional theory (DFT) calculations. Specifically, we estimated the transition states (TSs) for the aminolysis of α,α-difluoroacetates using nudged elastic band (NEB) calculations[23] at DFT level and subsequent transit-guided quasi-Newton[24] calculations for methylamine and methyl α,α-difluoro-α-phenylacetate as simplified prototype reactants. In fact, the obtained mechanistic insights into the aminolysis reaction enabled establishing a successful reaction condition for aminolysis postpolymerization modification. Despite this successful integration of computational chemistry with polymer synthesis, some problems still remain to be solved. As discussed above, the use of the NEB method enables facile access to TS geometries. However, the computational cost is high because the NEB method conducts numerous iterative calculations on the discretization points, the so-called images,

generated between reactants and products, thereby converging into rough TS structures. In general, NEB calculations involve hundreds of energy calculations in total. Therefore, NEB computations at the DFT level can be only applied to simplified model reactants. This computational limitation results in two drawbacks. First, the comparison of similar reactants is practically limited because DFT calculations are computationally demanding; DFT-determined energies are sensitive to functionals/basis sets even though the DFT-determined geometries are robust, thereby requiring case-by-case analysis regarding reaction energies. Second, the reaction profiling for aminolysis postpolymerization modification needs to be conducted on simplified prototype reactants consisting of only a few dozen atoms to reduce the computational cost. Therefore, to provide a useful compass for activated ester–amine chemistry in polymer synthesis, a computational guideline for a series of activated esters and realistic model reactants containing more than a hundred atoms should be constructed.

In this context, the use of semiempirical quantum mechanical (SQM) calculations can be envisaged as an important option to reduce the computational cost. However, classical SQM models are obtained by approximating Hartree–Fock (HF) models and thus inherit the weakness of the parent HF models. Unfortunately, the reduction in the computational cost sacrifices the calculation accuracy, thereby failing to replace DFT-level calculations. Considering that DFT calculations have been the predominant choice over HF models in the past decades, it is not surprising that a DFT-derived SQM, the so-called density functional-based tight binding method, has been gathering increasing attention from the chemistry community. Very recently, the group of Grimme proposed a robust DFT-based SQM method, termed as GFN*n*-xTB (short for Geometry, Frequency, Noncovalent interactions, *n*th generation, extended Tight Binding), which offers an alternative to DFT-level computations, especially for geometry optimization

calculations.[25-27] Due to the reduced computational cost of the GFN*n*-xTB method, we envisioned that GFN*n*-xTB computations could provide fast-track access to reaction mechanism information, providing a deeper insight into the aminolysis reaction for postpolymerization modification. To the best of our knowledge, no study has utilized GFN*n*-xTB calculations to obtain computational insight into aminolysis postpolymerization modification reactions.

In this study, we first analyzed the computational utility of GFN*n*-xTB. Then, by exploiting the feasibility of the GFN*n*-xTB method, we performed a systematic comparison of a series of activated esters for aminolysis and a computational reaction profiling for realistic model reactants consisting of over a hundred atoms. With this work, we aim to provide a computational compass for aminolysis postpolymerization modification reactions by carefully comparing existing and new experimental results.

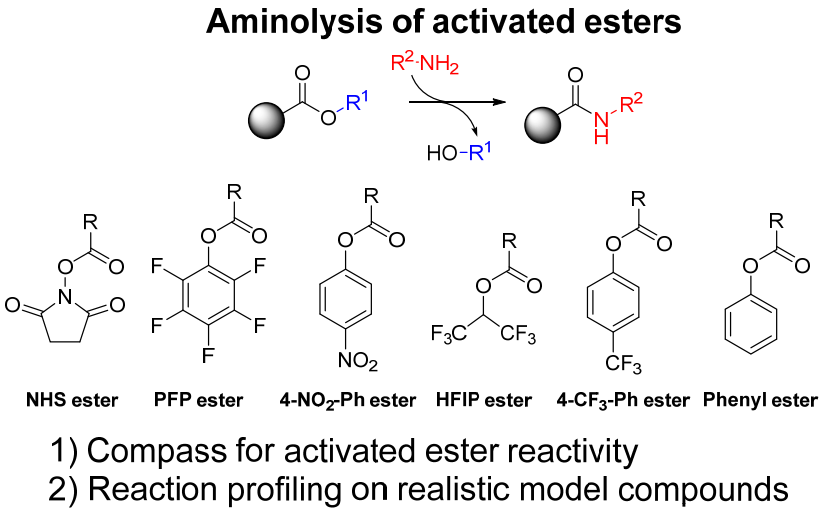

Scheme 1. Schematic overview of this work.

Results and Discussion

Low-cost computational analysis of the aminolysis of α,α-difluoro acetates

To gain robust and comprehensive insights into a series of activated esters for real postmodification reactions, we focused on reducing the computational cost of our previously reported NEB calculation on transition state (TS) structures for aminolysis postpolymerization modifications. To achieve this, we selected the ORCA software package due to the following three reasons:[28] First, ORCA features the state-of-the-art NEB implementation, the so-called energy-weighted climbing-image NEB, which enables TS prediction with reduced iterative calculations.[27] Second, by taking advantage of the built-in-interface to Grimme's GFN*n*-xTB SQM binaries, the calculations with GFN*n*-xTB can be directly conducted via ORCA. Third, ORCA features the domain-based local pair natural orbital coupled-cluster theory (DLPNO-CCSD(T)), which has been proven to be a good approximation for the golden standard canonical CCSD(T) calculations.[29] On the basis of these software characteristics, we aimed to gain fast-track access to reaction mechanism determination. To provide comparison with already published mechanistic information, we first conducted a computational analysis by employing methyl α,α-difluoro-α-phenylacetate (Ph-CF_2CO_2Me) and methylamine ($MeNH_2$) as prototype reactants. According to our previous computational study of the aminolysis of Ph-CF_2CO_2Me, two major mechanistic aspects need to be considered, i.e., a self-catalytic path involving a second amine molecule vs. a noncatalytic pathway and concerted vs. stepwise mechanisms, as summarized in Table 1. In the noncatalytic concerted aminolysis, the amine and ester reactants form an intermolecular hydrogen bonding ($Init_{non\_C}$) that provides stabilization in comparison with the infinitely separated amine–ester pair. Then, the amine attacks the ester carbonyl center, and the amine NH proton is then transferred to the leaving alkoxy fragment to form the amide structure via the transition state TS_{non_C}. In the noncatalytic stepwise aminolysis, the amine and ester reactants also interact via intermolecular hydrogen bonding ($Init_{non\_S}$). Then, the amine

nucleophilically attacks the ester to produce a hemiaminal intermediate (IM_{non_S}) via the transition state $TS1_{non\_S}$. Afterward, IM_{non_S} releases an alcohol to produce the desired amide product via the transition state $TS2_{non\_S}$. In self-catalytic processes, another amine molecule participates in the reaction as a proton transfer catalyst for the above two mechanisms. Therefore, we denoted the molecular states (initial hydrogen bonding and TS structures) corresponding to self-catalytic pathways as $Init_{cat\_C}$ and TS_{cat_C} for the self-catalytic concerted mechanism and $Init_{cat\_S}$, $TS1_{cat\_S}$, IM_{cat_S}, and $TS2_{cat\_S}$ for the self-catalytic stepwise mechanism. We will employ this terminology hereafter for the activated ester aminolysis.

Although the four possible reaction pathways need to be computed for the aminolysis of Ph-CF_2CO_2Me, we employed the noncatalytic concerted mechanism as the prototype reaction pathway to verify the efficiency and accuracy of the low-cost computations. We calculated the reaction energetics in the gas phase using the ORCA program. To construct the reaction energy profile, the reaction mechanism determination comprised the following four steps: 1) NEB calculations to determine the rough TS structures, followed by their optimization by eigenvector following method ($Calc_{NEB\_TS}$); 2) further TS optimization and frequency calculations ($Calc_{OPT-TS}$); 3) intrinsic reaction coordinate (IRC) calculations to connect the reactant and product structures via the TS structure ($Calc_{IRC}$); and 4) structure optimization of the reactant and product structures obtained in the IRC calculations ($Calc_{OPT}$). To validate the computational results obtained using the ORCA package, we first computed the abovementioned four steps ($Calc_{NEB\_TS}$, $Calc_{OPT-TS}$, $Calc_{IRC}$, and $Calc_{OPT}$) using the hybrid functional incorporating Becke's three-parameter exchange with the Lee, Yang, and Parr correlation functional[30, 31] (B3LYP) with the def2-SVP[32] basis set (entry 1, Table 1). Although we used the Pople-type double-zeta basis set (6-31G(d,p)) in our previous work, we selected here an equivalent double-zeta basis set, i.e.,

Ahlrichs-type def2-SVP, due to its high compatibility with the ORCA package in terms, for instance, of the resolution of the identity (RI) approximation technique. The resulting reaction energy profile was in good agreement with that obtained in our previous study. With the reference calculations in hand, we then tackled the reduction in the calculation cost for the reaction energy determination. Among the abovementioned four steps, $Calc_{NEB\_TS}$ and $Calc_{IRC}$ are highly computational demanding. Since $Calc_{NEB\_TS}$ is a crucial step in this study, we subjected it to SQM calculations using Grimme's GFN2-xTB (entry 2, Table 1). To verify the accuracy of the TS structure obtained at the GFN2-xTB level of theory, we used the resulting TS structure as a seed structure for TS determination at the B3LYP/def2-SVP level of theory with good results. Subsequent $Calc_{IRC}$ and $Calc_{OPT}$ calculations led to a reaction energy profile that was in excellent agreement with the DFT-only calculations (entry 1, Table 1). These successful geometry calculations at the GFN2-xTB level of theory motivated us to further reduce the computational cost by conducting the $Calc_{IRC}$ step at the GFN2-xTB level of theory (entry 3, Table 1), wherein only structure optimization calculations at DFT level for reactant, TS, and product were required to determine the reaction mechanism. As expected, the GFN2-xTB level of theory provided accurate geometries that could be employed as the initial guess for DFT level calculations. Thus, the computationally demanding steps $Calc_{NEB\_TS}$ and $Calc_{IRC}$ were now feasible with the GFN2-xTB level of theory, and only the $Calc_{OPT\text{-}TS}$ and $Calc_{OPT}$ steps were computed at the DFT level, thereby drastically reducing the computational cost without sacrificing the accuracy. For example, the GFN2-xTB method allowed accelerating the $Calc_{NEB\_TS}$ step at the B3LYP/def2-SVP level by 82 times. Of note, when we computed the four steps at the GFN2-xTB level of theory (entry 4, Table 1), the energetic accuracy was compromised compared with the result described in entry 3, Table 1. These computational

results demonstrated that the latter condition (entry 3, Table 1) provided the best balance between computational cost and accuracy. Therefore, we used it as the default calculation procedure in this study.

Table 1. Ab initio results[a] of the noncatalytic stepwise pathway for the aminolysis of Ph-CF_2CO_2Me and $MeNH_2$

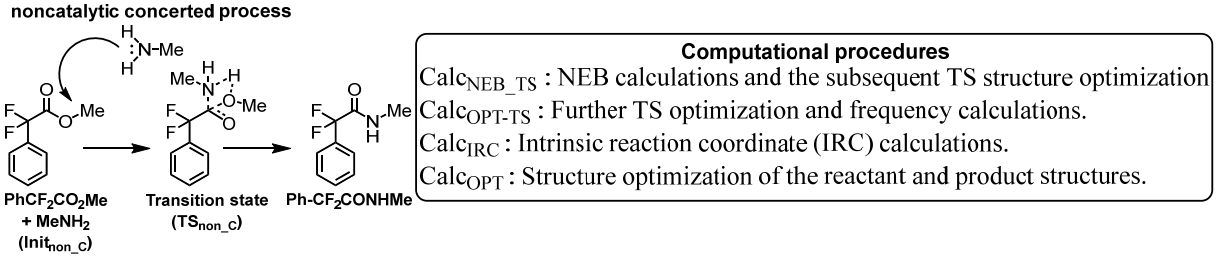

entry	1st process	2nd process	3rd process	4th process	ΔE ($Init_{non\_C}$)	ΔE (TS_{non_C})
1	$Calc_{NEB\_TS}$ B3LYP/def2-SVP	$Calc_{OPT\text{-}TS}$ B3LYP/def2-SVP	$Calc_{IRC}$ B3LYP/def2-SVP	$Calc_{OPT}$ B3LYP/def2-SVP	−5.6	32.9
2	$Calc_{NEB\_TS}$ GFN2-xTB	$Calc_{OPT\text{-}TS}$ B3LYP/def2-SVP	$Calc_{IRC}$ B3LYP/def2-SVP	$Calc_{OPT}$ B3LYP/def2-SVP	−5.6	32.8
3	$Calc_{NEB\_TS}$ GFN2-xTB	$Calc_{IRC}$ GFN2-xTB	$Calc_{OPT\text{-}TS}$ B3LYP/def2-SVP	$Calc_{OPT}$ B3LYP/def2-SVP	−5.5	32.8
4	$Calc_{NEB\_TS}$ GFN2-xTB	$Calc_{OPT\text{-}TS}$ GFN2-xTB	$Calc_{IRC}$ GFN2-xTB	$Calc_{OPT}$ GFN2-xTB	−6.8	25.8
ref[b]	$Calc_{NEB\_TS}$ B3LYP/6-31G**	$Calc_{OPT\text{-}TS}$ B3LYP/6-31G**	$Calc_{IRC}$ B3LYP/6-31G**	$Calc_{OPT}$ B3LYP/6-31G**	−4.9	33.9

[a] The energies (ΔE) are given in kcal·mol^{-1} with respect to the reactant state ($Init_{non\_C}$). For all the B3LYP/def2-SVP calculations, the resolution of the identity approximation was applied.
[b] Reported in ref. 21.

Having optimized the calculation procedure, we verified the robustness and feasibility of the computational approach by computing the remaining three reaction mechanisms, namely, the noncatalytic stepwise, self-catalytic concerted, and self-catalytic stepwise reaction mechanisms, using the optimized low-cost calculations as summarized in Table 2. As expected, the four reaction mechanisms could be feasibly determined, and the obtained energy profiles were in good accord with the previously reported profile that was conducted exclusively at the DFT level.

Table 2. Low-cost computation results[a,b] for the transition states of the aminolysis of methyl α, α-difluoroacetate by methylamine

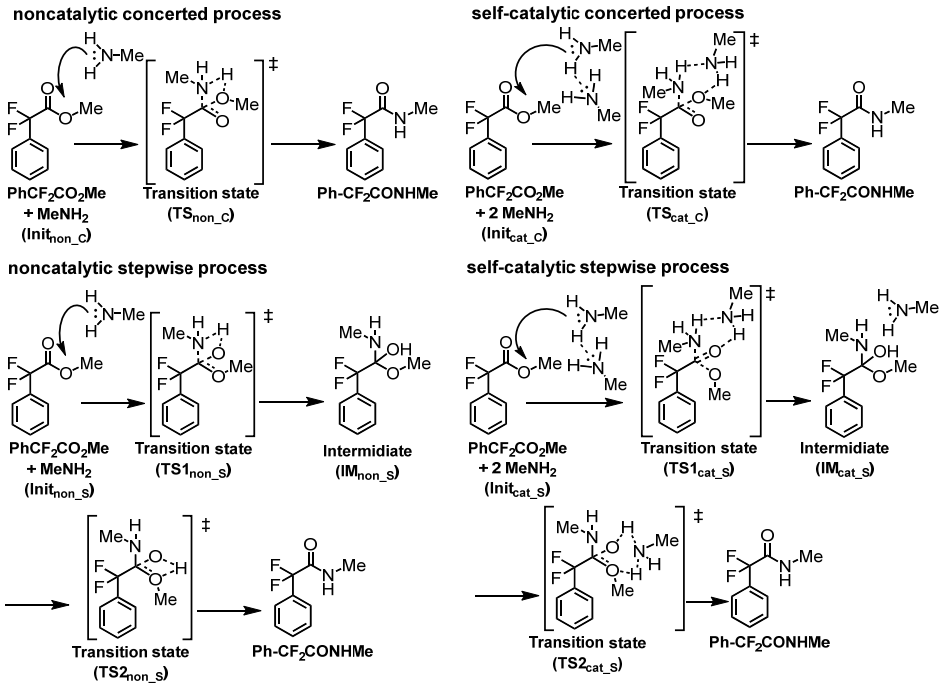

Reaction mechanism	noncatalytic concerted	noncatalytic stepwise		self-catalytic concerted	self-catalytic stepwise	
	TS_{non_C}	$TS1_{non\_S}$	$TS2_{non\_S}$	TS_{cat_C}	$TS1_{cat\_S}$	$TS2_{cat\_S}$
This work	32.8	37.2	35.1	20.4	17.5	21.0

Reference energy diagram for the Ph-CF_2CO_2Me aminolysis[c]						
B3LYP/6-31G(d,p)[c]	33.9	38.2	35.0	22.4	17.6	21.9

[a] The energies (ΔE) are given in kcal·mol^{-1} with respect to the reactant state (Init) in each mechanism.
[b] The energy of TS2 with respect to the hemiaminal intermediate (IM) for the stepwise mechanisms is given in parentheses.
[c] Reported in ref. 21.

Monomer design via a comprehensive analysis of activated ester aminolysis

As explained above, the reduced computational cost allowed performing fast-track reaction mechanism estimations. We then conducted a comprehensive comparison of commonly used activated esters to provide a feasible compass for the design of activated ester monomers. Since DFT-determined energies are susceptible to employed functionals/basis set combinations, the direct comparison of energy profiles between similar reaction systems requires case-by-case analysis. In this context, we employed the DLPNO-CCSD(T) method for single-point energy calculations to determine the absolute reaction energy profiles because post-HF methods, including the CCSD(T) method, are essentially free from semiempirical parameterization, ensuring the comparison among different reactants would be robust. It should be noted that the DLPNO-CCSD(T) method can afford canonical CCSD(T) level accuracy with a cost comparable to that of DFT calculations, thereby providing access to CCSD(T) level computations even with standard computational facilities. Considering this background, we selected four activated ester motifs used in polymer science, including *N*-hydroxysuccinimide acetate (NHS-Ac), pentafluorophenyl acetate (PFP-Ac), 4-nitrophenyl acetate (4-NO_2-Ph-Ac), and hexafluoroisopropyl acetate (HFIP-Ac). In addition, we employed 4-trifluoromethylphenyl acetate (4-CF_3-Ph-Ac) and phenyl acetate (Ph-Ac) as control ester compounds. Along with the ester components, we selected methylamine as a model reactant. We started the activated ester

comparison with the widely used conventional activated ester NHS-Ac (Figures 1 and 2), analyzing the four mechanisms (noncatalytic concerted, noncatalytic stepwise, self-catalytic concerted, and self-catalytic stepwise mechanisms) of the aminolysis reaction at the DLPNO-CCSD(T) level in both gas and tetrahydrofuran (THF; conductor-like polarizable continuum model, CPCM[33]) using the cc-pVTZ basis set, as summarized in Table 3. We found two interesting results. First, no TS structures were located for the self-catalytic mechanisms. Second, the reaction energy barrier of the noncatalytic concerted pathway (ΔE = 23.9 kcal·mol^{-1}) was 10.4 kcal·mol^{-1} lower than that of the noncatalytic stepwise mechanism and comparable with that of the self-catalytic aminolysis of α,α-difluoroacetate esters. These calculation results showed that NHS-Ac aminolysis reactions proceed most likely via the noncatalytic concerted pathway, which can be explained in terms of the chemical nature of the NHS moiety. Specifically, the formation of hemiaminal structures would be unfavorable because the *N*-hydroxysuccinimide leaving groups would coexist with the intramolecular hydroxyl nucleophile. In addition, the 1:1 ester-to-amine reaction is accessible, and thus the participation of a second amine molecule in the aminolysis would increase the polarity of the TS structures, blocking the self-catalytic concerted and stepwise mechanisms.

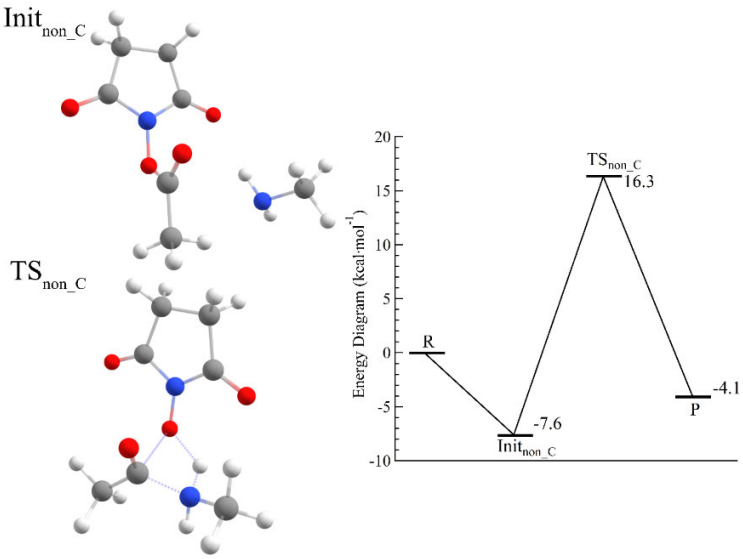

Figure 1. Energy diagram of the noncatalytic concerted mechanism for the aminolysis of *N*-hydroxysuccinimide acetate by methylamine calculated at the DLPNO-CCSD(T)/cc-pVTZ// B3LYP/def2-SVP level of theory in gas phase. The color code is as follows: O, red; N, blue; C, gray; H, white.

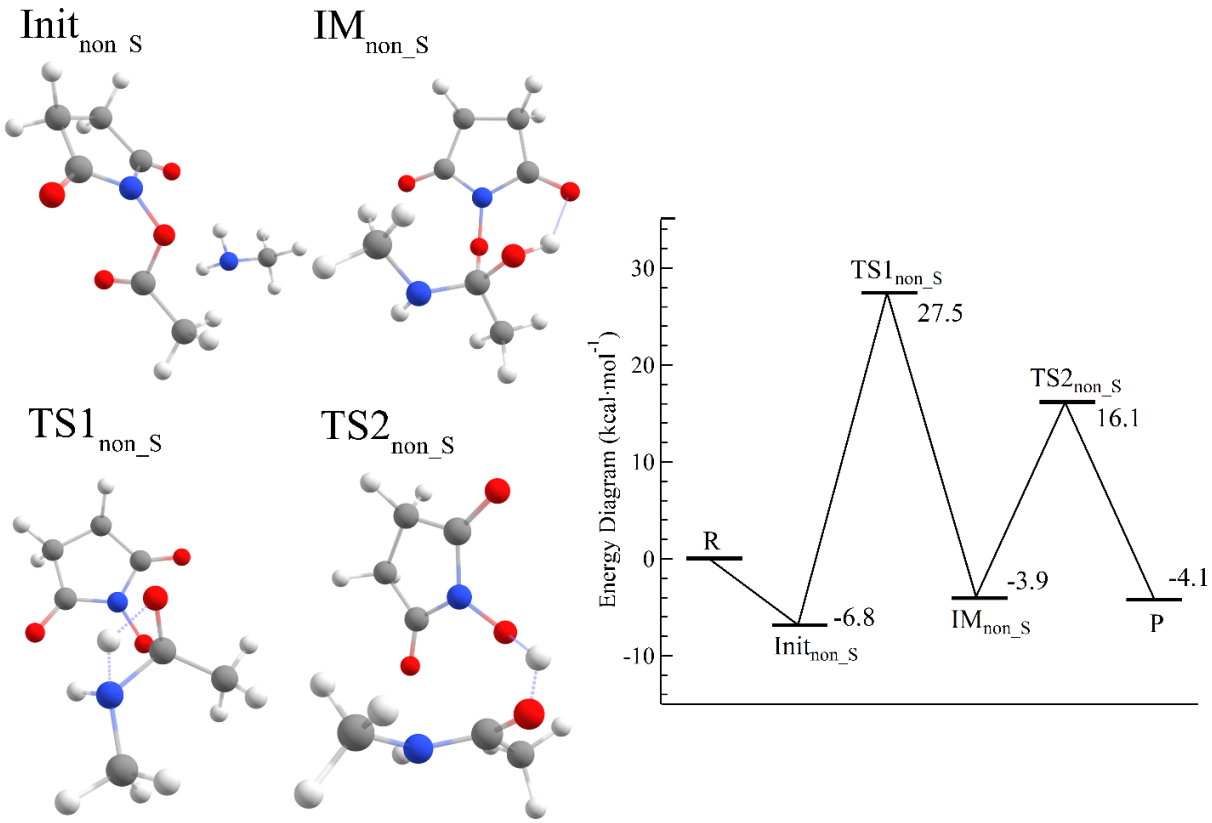

Figure 2. Energy diagram of the noncatalytic stepwise mechanism for the aminolysis of *N*-hydroxysuccinimide acetate by methylamine calculated at the DLPNO-CCSD(T)/cc-pVTZ// B3LYP/def2-SVP level of theory in gas phase. The color code is as follows: O, red; N, blue; C, gray; H, white.

Table 3. DLPNO-CCSD(T) results[a] for the transition states of the aminolysis of *N*-hydroxysuccinimide acetate by methylamine

Reaction mechanism	noncatalytic concerted	noncatalytic stepwise		self-catalytic concerted	self-catalytic stepwise	
	TS_{non_C}	$TS1_{non\_S}$	$TS2_{non\_S}$	TS_{cat_C}	$TS1_{cat\_S}$	$TS2_{cat\_S}$

gas phase	23.9	34.3	23.0	-[b]	-[b]	-[b]
in THF[c]	15.4	31.2	17.9	-[b]	-[b]	-[b]

[a] The energies (ΔE) are given in kcal·mol^{-1} with respect to the reactant state (Init) in each mechanism. All energy profiles were calculated at the DLPNO-CCSD(T)/cc-pVTZ level of theory on the structures optimized at the B3LYP/def2-SVP level.
[b] The TS structures were not located.
[c] The solvation effect was considered using the CPCM method implemented in ORCA.

The results of the estimation of the noncatalytic concerted and stepwise mechanisms for the other esters are summarized in Table 4 (detailed computational results are provided in Figures S1–10 in the supporting information). As expected, the commonly used activated esters NHS-Ac, PFP-Ac, and 4-NO_2-Ph-Ac showed very similar reaction profiles regardless of the ester structures, with an activation energy for the aminolysis via the noncatalytic concerted pathway of around 25 kcal·mol^{-1} in gas phase and 15 kcal·mol^{-1} in THF. These results are in accord with the feasible reactivity in postpolymerization modification reactions of the three activated esters. In sharp contrast, the activation energy for the Ph-Ac aminolysis (22.2 kcal·mol^{-1} in THF) was about 5–9 kcal·mol^{-1} higher than that for the reaction with the three esters, which is in good agreement with the limited aminolysis postpolymerization modification reactivity of polymers featuring phenyl esters.[34] Furthermore, this computational comparison at the DLPNO-CCSD(T) level of theory explained well the aminolysis behavior of HFIP-Ac. Specifically, Nuhn, Zentel, and coworkers reported that poly(hexafluoroisopropyl methacrylate)s can undergo aminolysis postpolymerization modification with high ester conversions only when a large excess of primary amine (50 eq. to esters) is employed at 65 °C.[18] This result is in accord with our computations at the DLPNO-CCSD(T) level of theory, according to which the activation energy for the HFIP-Ac aminolysis (20.2 kcal·mol^{-1} in THF) was considerably higher than that for the

aminolysis of standard activated esters (NHS-Ac, PFP-Ac, and 4-NO_2-Ph-Ac) but lower than that of the stable ester Ph-Ac. During this study, we found that the activation energy for the 4-CF_3-Ph-Ac aminolysis (17.8 kcal·mol^{-1} in THF) was similar to that for the reaction of NHS-Ac and PFP-Ac, which strongly indicated that 4-trifluoromethylphenyl esters might serve as feasible activated esters in the same manner to the well-established PFP and NHS esters. Although polymers featuring 4-trifluoromethylphenyl esters were prepared and preliminarily subjected to aminolysis postmodification, no detailed mechanistic insights were reported.[35] Therefore, we synthesized poly(4-trifluoromethylphenyl acrylate) (PA-4-CF_3-Ph) and performed prototype aminolysis postpolymerization modification with 1.1 equivalent of *n*-hexylamine in 1,4-dioxane at 80 °C for 4 h. Characterization of the resultant product by means of Fourier transform infrared (FT-IR) spectroscopy, ^{1}H nuclear magnetic resonance (NMR) spectroscopy, and size exclusion chromatography (SEC) measurements (Figures 3–5) revealed that the polymeric activated esters were obtained with an ester conversion of 84.2%. The reaction progress was supported by the appearance of a strong peak at 1639 cm^{-1} due to the amide C = O and a significant decrease in the intensity of the peak corresponding to the stretching vibration of the ester bond at 1752 cm^{-1} in the FT-IR spectrum of the polymers recovered after the aminolysis (Figure 3). This was further confirmed by the ^{1}H NMR result, which showed a peak attributable to the hexylamide residue at 0.7–1.6 ppm, whereas those of the ester residue at 7.0–7.9 ppm decreased (Figure 4). Moreover, we found no evidence of side reactions including decomposition or crosslinking according to the SEC results of the polymers before and after the aminolysis (Figure 5). These results demonstrate that the computations based on the GFN2-xTB and DLPNO-CCSD(T) methods provided a rational prediction of real experiments.

Table 4. Computational results[a] at DLPNO-CCSD(T)/cc-pVTZ//B3LYP/def2-SVP for the transition states of the ester aminolysis with methylamine

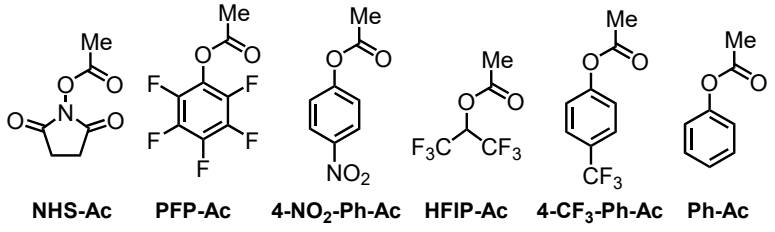

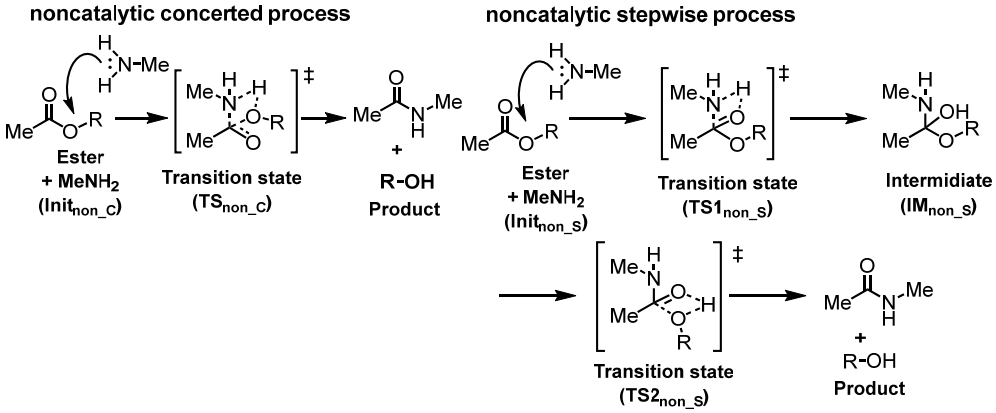

ester	noncatalytic concerted		noncatalytic stepwise			
	TS_{non_C} (gas)	TS_{non_C} (THF[c])	$TS1_{non\_S}$ (gas)	$TS2_{non\_S}$ (gas)	$TS1_{non\_S}$ (THF[c])	$TS2_{non\_S}$ (THF[c])
NHS-Ac	23.9	15.4	34.3	23.0	31.2	17.9
PFP-Ac	21.9	13.2	36.4	17.5	32.4	11.3
4-NO_2-Ph-Ac	25.6	14.8	35.8	18.5	30.7	11.1
HFIP-Ac	28.3	20.2	36.2	25.0	32.4	21.5
4-CF_3-Ph-Ac	27.6	17.8	37.7	22.7	33.3	16.5
Ph-Ac	31.2	22.2	39.0	26.0	34.6	20.4

[a] The energies (ΔE) are given in kcal·mol^{-1} with respect to the reactant state (Init) in each mechanism.

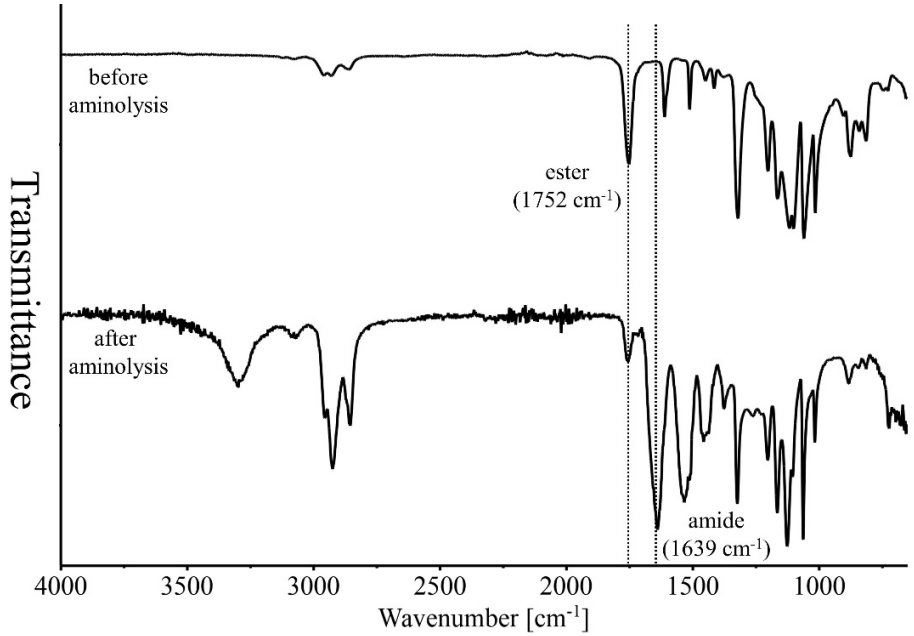

Figure 3. Attenuated total reflectance Fourier transform infrared spectra of poly(4-trifluoromethylphenyl acrylate) before (top) and after (bottom) aminolysis with 1.1 equivalents of *n*-hexylamine.

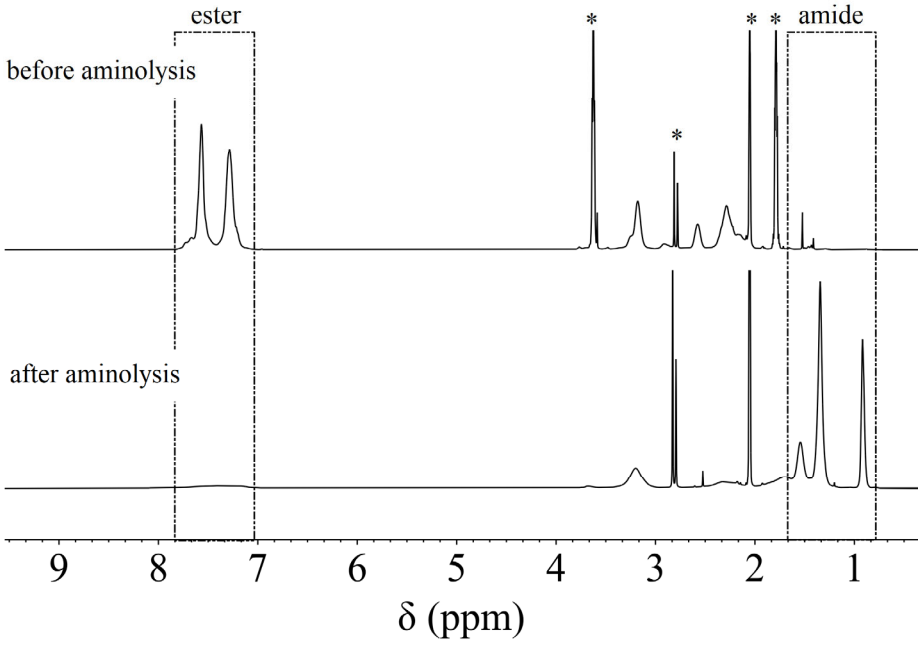

Figure 4. ^{1}H nuclear magnetic resonance spectra in acetone-d_6 of poly(4-trifluoromethylphenyl acrylate) before (top) and after (bottom) aminolysis with 1.1 equivalents of *n*-hexylamine (the asterisk denotes the signals of residual solvent).

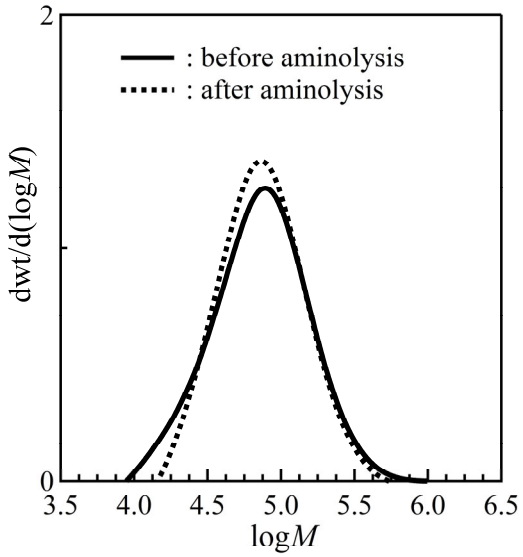

Figure 5. Size exclusion chromatography traces of poly(4-trifluoromethylphenyl acrylate) before and after aminolysis with 1.1 equivalents of *n*-hexylamine.

Reaction profiling of the aminolysis postpolymerization modification using realistic model compounds

To demonstrate the utility of the present low-cost computations, we applied them to determine the reaction profile of realistic model compounds. Generally, computational reaction profiling requires extensive simplification of the reaction system to reduce the calculation costs. This is achieved in this study by integrating the GFN2-xTB method, which is particularly important for polymer chemistry because only fragment structures of polymers are usually subjected to high-level theory calculations due to the high number of atoms comprising the polymers. We computationally analyzed our recent results on the aminolysis postpolymerization modification

of polymers featuring α,α-difluoroacetates. In brief, we synthesized an α,α-difluoroacetate-containing polymer (poly-CF_2CO_2Et) via Friedel–Crafts polycondensation between 1,4-dimethoxybenzene and 4-OHC-C_6H_4-CF_2CO_2Et and subjected the resulting polymer to aminolysis postpolymerization modification with amines. Specifically, the reaction with *n*-hexylamine afforded a 100% ester conversion in the postpolymerization step to provide the corresponding aminolyzed product.[21, 22] As a proof of concept, we computationally analyzed this postpolymerization modification reaction using a realistic model structure consisting of a hexameric sequence (oligo-CF_2CO_2Et) and *n*-hexylamine as a reactant. We computed the four possible reaction pathways without further approximations such as ONIOM,[36] as depicted in Figures 6–9, and calculated the final reaction profiles at the DLPNO-CCSD(T) level of theory to gain an absolute insight into the reactivity. The results are summarized in Table 5. Unlike the computations for small molecules, structure convergence can be a decisive factor for large molecules. Therefore, we conducted all the structure optimization calculations for large molecules by gradually increasing the calculation levels on the basis of Grimme's composite electronic structure methods, which can afford good calculation results with low computational cost compared with standard calculations. First, we optimized the structures obtained from NEB calculations at the GFN2-xTB level of theory at Grimme's HF-based HF-3c[37] and then at Grimme's DFT-based r^{2}SCAN-3c[38] level of theory. As in the case of small molecules, we computed all the reaction pathways and obtained the corresponding reactant, TS, and product structures with a realistic large model compound. Then, we obtained a preliminary insight into the polymer effect during the aminolysis postpolymerization modification reactions by varying the initial amine nucleophile geometry. To this aim, we computed the noncatalytic concerted reaction with and without considering the polymer effects as shown in Figure 10, finding that the

activation energy for the reaction path in the former case was 7.2 kcal·mol^{-1} higher than that obtained in the latter. Interestingly, the activation energy increased due to an additional stabilization of the initial amine–polymer noncovalent interactions, which could explain the fact that postpolymerization modification reactions often suffer from incomplete consumption of the polymeric reactants. The decreased postmodification reactivity at the last stage of the reactions could be attributed to the increased stabilization of the reactant through interactions with the polymer chains. Although it was out of the scope of this study, this entanglement with reactants could be an important factor in postpolymerization modification reactions to be analyzed at the DLPNO-CCSD(T) level of theory.

These results demonstrate that reaction information for large molecular systems, including the polymer effect during postpolymerization modifications, can be obtained even at the DLPNO-CCSD(T) level of theory by taking advantage of the ORCA software package without requiring additional approximations such as ONIOM.

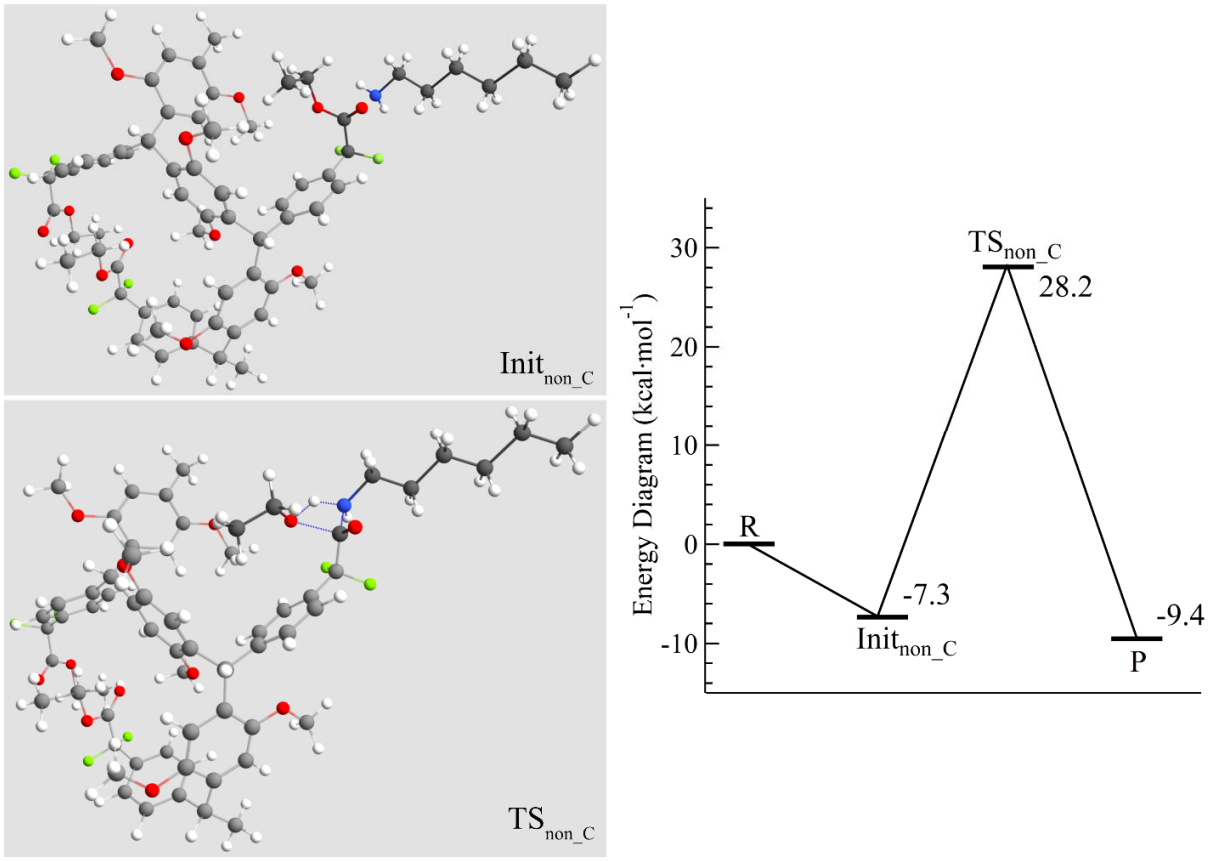

Figure 6. Energy diagram of the noncatalytic concerted mechanism for the aminolysis of oligo-CF_2CO_2Et by *n*-hexylamine calculated at the DLPNO-CCSD(T)/cc-pVTZ//r^{2}SCAN-3c level of theory in gas phase. The color code is as follows: O, red; N, blue; C, gray; F, green; H, white.

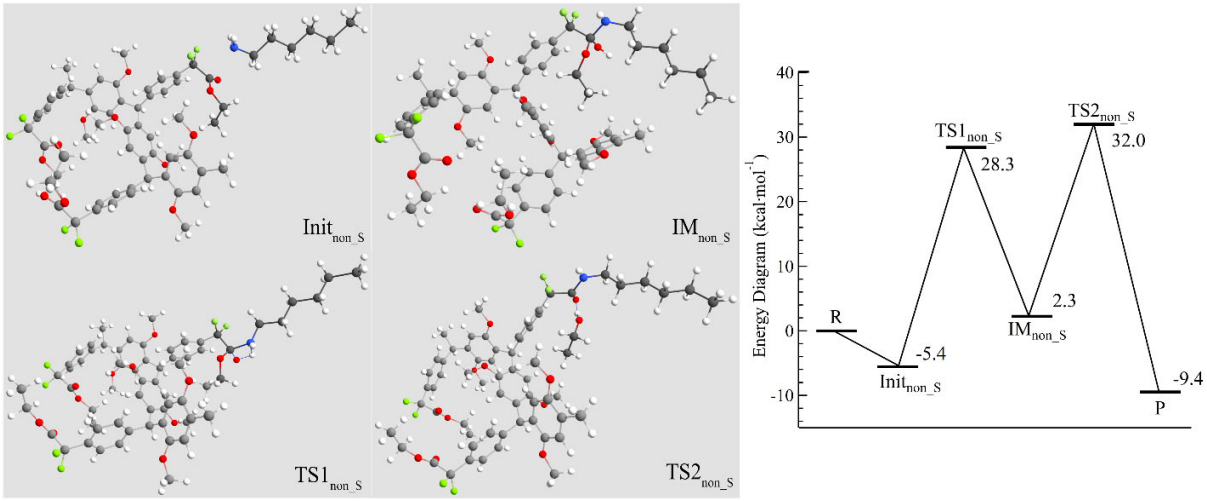

Figure 7. Energy diagram of the noncatalytic stepwise mechanism for the aminolysis of oligo-CF_2CO_2Et by *n*-hexylamine calculated at the DLPNO-CCSD(T)/cc-pVTZ//r^{2}SCAN-3c level of theory in gas phase. The color code is as follows: O, red; N, blue; C, gray; F, green; H, white.

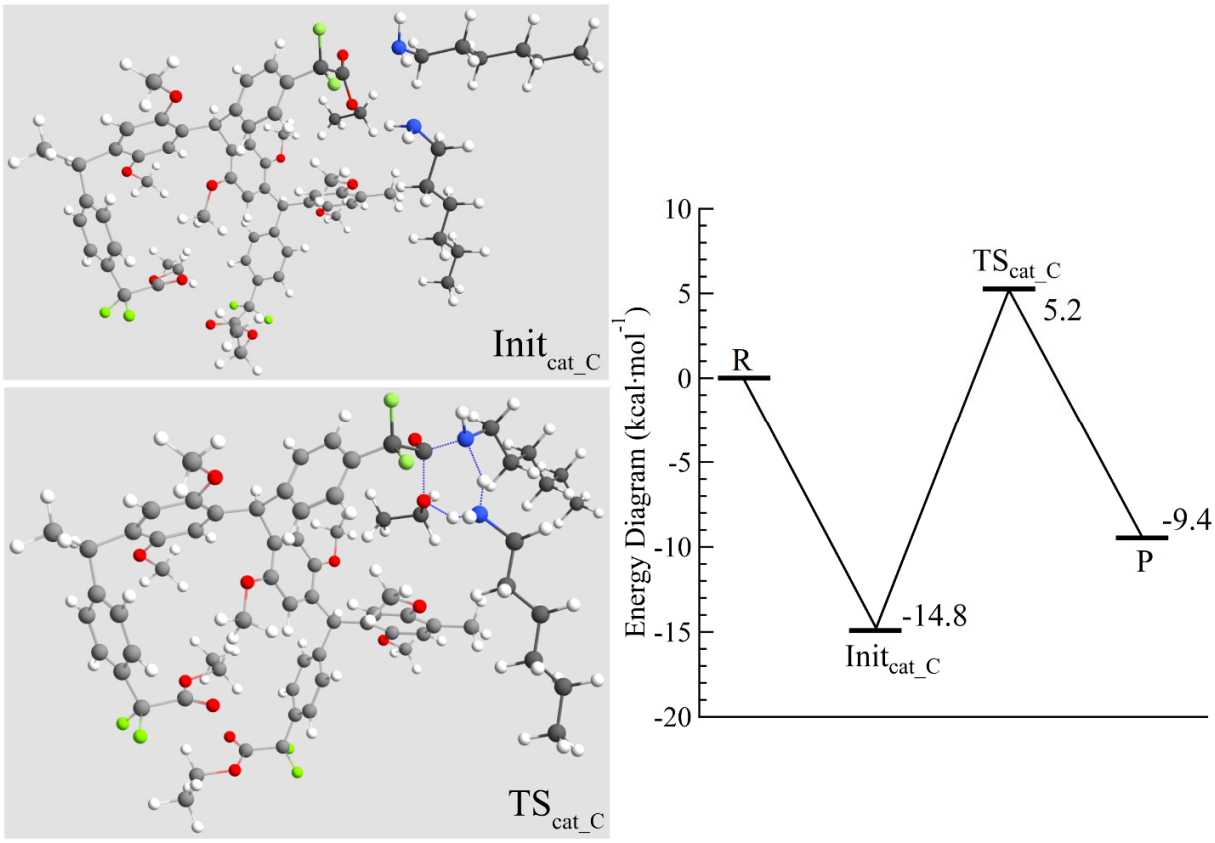

Figure 8. Energy diagram of the self-catalytic concerted mechanism for the aminolysis of oligo-CF_2CO_2Et by *n*-hexylamine calculated at the DLPNO-CCSD(T)/cc-pVTZ//r^{2}SCAN-3c level of theory in gas phase. The color code is as follows: O, red; N, blue; C, gray; F, green; H, white.

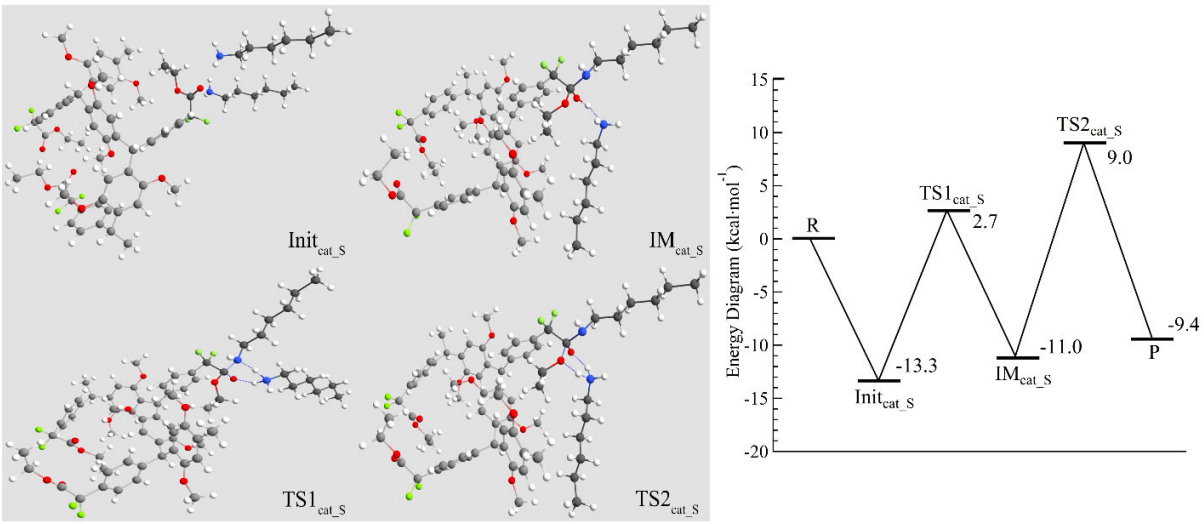

Figure 9. Energy diagram of the self-catalytic stepwise mechanism for the aminolysis of oligo-CF_2CO_2Et by *n*-hexylamine calculated at the DLPNO-CCSD(T)/cc-pVTZ//r^{2}SCAN-3c level of theory in gas phase. The color code is as follows: O, red; N, blue; C, gray; F, green; H, white.

Table 5. Ab initio results[a,b] for the transition states of the aminolysis of oligo-CF_2CO_2Et by *n*-hexylamine

Reaction mechanism	noncatalytic concerted	noncatalytic stepwise		self-catalytic concerted	self-catalytic stepwise	
	TS_{non_C}	$TS1_{non\_S}$	$TS2_{non\_S}$	TS_{cat_C}	$TS1_{cat\_S}$	$TS2_{cat\_S}$
r^{2}SCAN-3c	30.6	33.8	31.2	18.2	15.0	19.4
DLPNO-CCSD(T)/cc-pVTZ //r^{2}SCAN-3c	35.5	33.7	37.4	20.0	16.0	22.4

[a] The energies (ΔE) are given in kcal·mol^{-1} with respect to the reactant state (Init) in each mechanism.
[b] The energy of TS2 with respect to the hemiaminal intermediate (IM) for the stepwise mechanisms is given in parentheses.
[c] Reported in ref. 11.

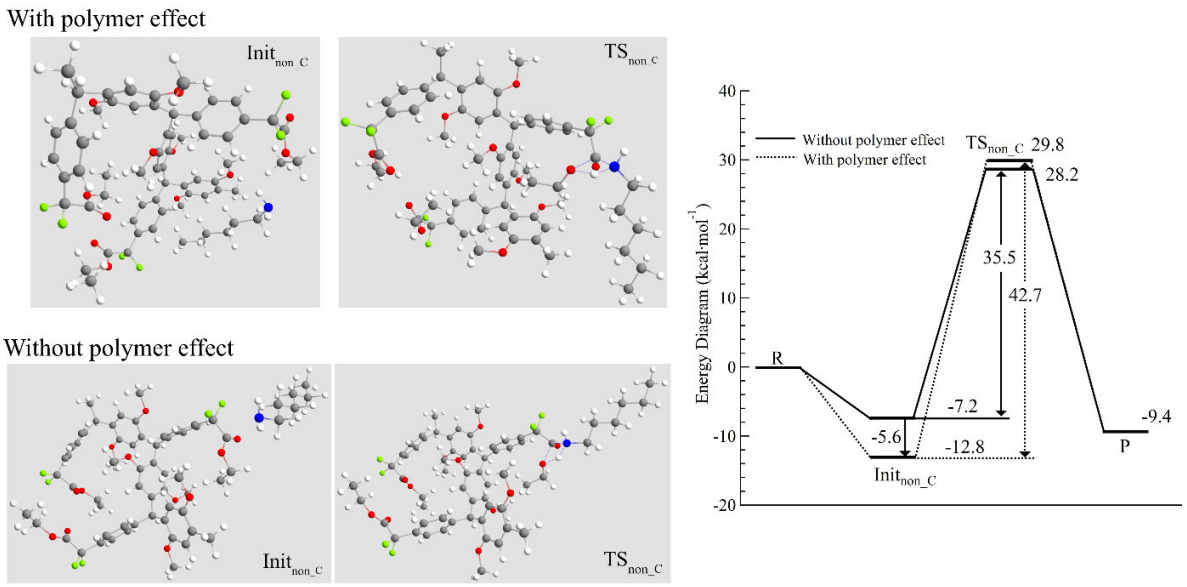

Figure 10. Energy diagram of the noncatalytic concerted mechanism for the aminolysis of oligo-CF_2CO_2Et by *n*-hexylamine with and without considering the polymer effect calculated at the DLPNO-CCSD(T)/cc-pVTZ//r^{2}SCAN-3c level of theory in gas phase. The color code is as follows: O, red; N, blue; C, gray; F, green; H, white.

Conclusions

In this work, we computationally analyzed the aminolysis behavior of activated esters by taking advantage of the fast and robust semiempirical method GFN2-xTB. Using the GFN2-xTB and DLPNO-CCSD(T) methods allowed us to predict the reactivity trends of a series of activated esters as compared with experimental observations. In brief, the activation energy barrier of NHS, PFP, and 4-nitrophenyl esters was considerably lower than that of HFIP and phenyl esters, demonstrating that HFIP and phenyl esters are not suitable candidates for postpolymerization modifications. Of note, the activation energy barrier for the aminolysis of the HFIP ester was

lower than that for phenyl esters, which is in agreement with the experimental fact that the aminolysis postmodification reactions of poly(hexafluoroisopropyl methacrylate)s require a large excess of primary amines (50 eq. to ester units). During this study, we found that the reactivity of a 4-trifluoromethylphenyl ester was similar to that of NHS, PFP, and 4-nitrophenyl esters, suggesting that it could be subjected to postmodification reactions. Thus, we subjected the newly synthesized PA-4-CF_3-Ph ester to aminolysis postpolymerization reaction, which proceeded with high efficiency as predicted. In addition, we conducted TS estimations using realistic model compounds consisting of more than a hundred atoms. Unlike conventional DFT calculations, the GFN2-xTB method enabled constructing a reaction profiling with large molecules even at the DLPNO-CCSD(T) level of theory without requiring access to a supercomputer calculation center. Moreover, the realistic reaction profiling allowed us to perform a preliminary assessment and visualization of the polymer effect during the aminolysis postpolymerization modification. According to these results, we envision that the computational power of the GFN2-xTB and DLPNO-CCSD(T) methods will find practical application in polymer science.

Experimental

Materials

All chemicals used for synthesis were commercially available and used without further purification unless otherwise stated.

Instruments

All the ^{1}H and ^{13}C NMR spectra in deuterated solvents were recorded on a Brucker 500 MHz FT-NMR spectrometer, and the chemical shifts (δ) are given in ppm using either the solvent peak or tetramethylsilane as the internal standard. The SEC measurements were performed at 40 °C

and a flow rate of 1.0 mL·min^{-1} in dimethylformamide (DMF) containing 10 mmol·L^{-1} LiCl on a Waters gel permeation chromatography e2695 system embedded with two columns (7.8 × 300 mm Styragel HR 4E and 5E columns). The number-average molecular weight (M_n) and polydispersity ($Đ$) values of the polymers were calculated with polystyrene calibration. The standard IR spectra were recorded using an Agilent Cary 630 spectrometer equipped with an attenuated total reflectance unit. The products were purified using a single-channel automated flash chromatography system (Smart Flash EPCLC AI-580S, Yamazen). The optimized solvent condition for the column purification was determined using an EPCLC AI-580S system.

Synthesis

A-4-CF$_3$-Ph: A THF (30.9 mL) solution of 4-trifluoromethylphenol (2.0 g, 12.3 mmol) and NEt$_3$ **(**2.6 mL, 18.5 mmol) was degassed with Ar in an ice bath. To this solution, acryloyl chloride (1.5 mL, 18.5 mmol) was added dropwise. After the reaction mixture was stirred for 1 h at room temperature, the reaction solvent was diluted with ethyl acetate, and the obtained solution was washed with water. The recovered organic phase was distilled off under reduced pressure to afford a crude product, which was purified by column chromatography to afford the target A-4-CF$_3$-Ph as a transparent liquid.

Yield: 2.2 g (81.4%). ^{1}H NMR (500 MHz, CDCl$_3$) δ 7.67 (d, J = 8.5 Hz, 2H), 7.27 (d, J = 8.5 Hz, 2H), 6.64 (d, J = 17.5 Hz, 1H), 6.33 (dd, J = 10.5, 17.5 Hz, 1H), 6.06 (d, J = 10.5 Hz, 1H). ^{13}C NMR (126 MHz, CDCl$_3$) δ 163.95, 153.12, 133.35, 128.15 (q, J = 32.8 Hz), 127.45, 126.80 (q, J = 3.8 Hz), 124.97 (q, J = 272.0 Hz), 122.07.

Free-radical polymerization of A-4-CF$_3$-Ph: A 1,4-dioxane (3.9 mL) solution of A-4-CF$_3$-Ph (1.7 g, 7.9 mmol) and α,α′-azobis(isobutyronitrile) (25.8 mg, 0.16 mmol) was degassed in an Ar

atmosphere and then stirred at 70 ºC overnight. After the reaction completion, the crude product was purified by precipitation into hexane, yielding the target polymer PA-4-CF_3-Ph.

Yield: 1.7 g (quantitative); M_n (SEC, DMF): 55 kg mol^{-1}; $Đ$: 1.7.

Typical procedure for the postpolymerization modification reaction of PA-4-CF_3-Ph: *n*-Hexylamine (51.5 mg, 0.5 mmol) was added to a 1,4-dioxane (2.3 mL) solution of PA-4-CF_3-Ph (100 mg, 0.46 mmol), and the reaction mixture was stirred at 80 ºC for 4 h. The obtained crude product was purified by dialysis in acetone.

Yield: 60.5 mg (84.2%); M_n (SEC, DMF): 60 kg mol^{-1}; $Đ$: 1.5.

Computational analysis

TS search: The initial input structures were optimized using an equilibrium conformer search engine implemented in the Spartan'18 or 20 software with the preset default density functional theory parameters.[39] The TS structures were searched using the NEB-TS option implemented in ORCA (version 5.0.1), which successively conducted a climbing image NEB calculation and the subsequent TS structure optimization by eigenvector following method. Regarding the GFN2-xTB calculations, the precompiled xtb binary (version 6.4.1) was used as downloaded. Frequency calculations were performed to confirm the TS structures. IRC calculations, connecting the TS to the desired reactants and products, were performed with ORCA (version 5.0.1). Finally, all reactant and product structures obtained from the IRC calculations were further optimized, and none of the resulting stable structures were found to have imaginary frequencies. For insight, additional single-point energy calculations were performed at the DLPNO-CCSD(T)/cc-pVTZ level on B3LYP/def2-SVP-optimized structures in ORCA. The solvation effect was considered using the CPCM model implemented in ORCA.

Calculations for large molecules: The initial structures of the hexameric units containing activated esters were searched and optimized using the equilibrium conformer search engine implemented in the Conformer-Rotamer Ensemble Sampling Tool (CREST, version 2.11.1) developed by the group of Grimme.[40, 41] The most stable conformer was determined using CREST at the GFN2-xTB level with preset default metadynamic simulation time. Next, the CREST-determined initial structures were further optimized at HF-3c[37] and then r^{2}SCAN-3c[38] levels of theory in ORCA. To avoid carbonyl isomerization issues, initial structures of the amide products were generated by manually substituting the ester units with amide units for the initial structures of the activated ester reactants. The TS structures were searched using the NEB-TS option, and the following IRC calculations were conducted with ORCA. Finally, all reactant and product structures obtained from the IRC calculations were further optimized at HF-3c and subsequently r^{2}SCAN-3c in ORCA, and none of the resulting stable structures were found to have imaginary frequencies. Additional single-point energy calculations were performed at the DLPNO-CCSD(T)/cc-pVTZ level on r^{2}SCAN-3c-optimized structures in ORCA.

Visualization and analysis of computational results: The ORCA output files were analyzed and visually presented using the Chemcraft program.[42]

ASSOCIATED CONTENT

Supporting Information. The following files are available free of charge: calculation results for PFP-Ac, 4-NO_2-Ph-Ac, HFIP-Ac, 4-CF_3-Ph-Ac, and Ph-Ac.

AUTHOR INFORMATION

Corresponding Authors

(R.K.) Tel: +81-27-730-1447. E-mail: kakuchi@gunma-u.ac.jp

Author Contributions

The manuscript was written through contributions of all authors. All authors have given approval to the final version of the manuscript.

Funding Sources

R. K. gratefully acknowledges the Leading Initiative for Excellent Young Researchers (LEADER) for the financial support. R. K. and H. A. also acknowledge the S-Membrane Project and the F-Materials Project at Gunma University for the financial support.

References

1. Lutz, J.-F., 1,3-Dipolar Cycloadditions of Azides and Alkynes: A Universal Ligation Tool in Polymer and Materials Science. *Angew. Chem. Int. Ed.* **2007,** *46* (7), 1018-1025, doi:10.1002/anie.200604050.
2. Fournier, D.; Hoogenboom, R.; Schubert, U. S., Clicking polymers: a straightforward approach to novel macromolecular architectures. *Chem. Soc. Rev.* **2007,** *36* (8), 1369-1380.
3. Franc, G.; Kakkar, A. K., "Click" methodologies: efficient, simple and greener routes to design dendrimers. *Chem. Soc. Rev.* **2010,** *39* (5), 1536-1544.
4. Golas, P. L.; Matyjaszewski, K., Marrying click chemistry with polymerization: expanding the scope of polymeric materials. *Chem. Soc. Rev.* **2010,** *39* (4), 1338-1354.
5. Hoyle, C. E.; Lowe, A. B.; Bowman, C. N., Thiol-click chemistry: a multifaceted toolbox for small molecule and polymer synthesis. *Chem. Soc. Rev.* **2010,** *39* (4), 1355-1387.
6. Becer, C. R.; Hoogenboom, R.; Schubert, U. S., Click Chemistry beyond Metal-Catalyzed Cycloaddition. *Angew. Chem. Int. Ed.* **2009,** *48* (27), 4900-4908, doi:10.1002/anie.200900755.
7. Stuparu, M. C.; Khan, A., Thiol-Epoxy “click” Chemistry: Application in Preparation and Postpolymerization Modification of Polymers. *J. Polym. Sci. Part A* **2016,** *54* (19), 3057-3070, doi:10.1002/pola.28195.
8. Das, A.; Theato, P., Activated Ester Containing Polymers: Opportunities and Challenges for the Design of Functional Macromolecules. *Chem. Rev.* **2016,** *116* (3), 1434-1495, doi:10.1021/acs.chemrev.5b00291.
9. Barner-Kowollik, C.; Du Prez, F. E.; Espeel, P.; Hawker, C. J.; Junkers, T.; Schlaad, H.; Van Camp, W., “Clicking” Polymers or Just Efficient Linking: What Is the Difference? *Angew. Chem. Int. Ed.* **2011,** *50* (1), 60-62, doi:10.1002/anie.201003707.
10. Iha, R. K.; Wooley, K. L.; Nyström, A. M.; Burke, D. J.; Kade, M. J.; Hawker, C. J., Applications of Orthogonal Click Chemistries in the Synthesis of Functional Soft Materials. *Chem. Rev.* **2009,** *109* (11), 5620-5686, doi:10.1021/cr900138t.

11. Chu, C.; Liu, R., Application of click chemistry on preparation of separation materials for liquid chromatography. *Chem. Soc. Rev.* **2011,** *40* (5), 2177-2188.
12. Batz, H. G.; Franzmann, G.; Ringsdorf, H., Model reactions for synthesis of pharmacologically active polymers by way of monomeric and polymeric reactive esters. *Angew. Chem. Int. Ed.* **1972,** *11* (12), 1103-4, doi:10.1002/anie.197211031.
13. Eberhardt, M.; Mruk, R.; Zentel, R.; Théato, P., Synthesis of Pentafluorophenyl(meth)acrylate Polymers: New Precursor Polymers for the Synthesis of Multifunctional Materials. *Eur. Polym. J.* **2005,** *41*, 1569, doi:https://doi.org/10.1016/j.eurpolymj.2005.01.025.
14. Nilles, K.; Theato, P., Synthesis and Polymerization of Active Ester Monomers Based on 4-Vinylbenzoic Acid. *Eur. Polym. J.* **2007,** *43*, 2901.
15. Théato, P.; Zentel, R., α,ω-Functionalized Poly-N-Isopropylacrylamides: Controlling the Surface Activity for Vesicle Adsorption by Temperature. *J. Colloid Interface Sci.* **2003,** *268*, 258.
16. Nilles, K.; Theato, P., RAFT Polymerization of Activated 4-Vinylbenzoates. *J. Polym. Sci., Part A* **2009,** *47*, 1696.
17. Rejmanovti, P.; Labsky, J.; Kopecek, J., Aminolyses of Monomeric and Polymeric 4-Nitrophenyl Esters of N-Methacryloylamino Acids. *Makromol. Chem.* **1977,** *178*, 2159.
18. Nuhn, L.; Overhoff, I.; Sperner, M.; Kaltenberg, K.; Zentel, R., RAFT-Polymerized Poly(hexafluoroisopropyl Methacrylate)s as Precursors for Functional Water-Soluble Polymers. *Polym. Chem.* **2014,** *5*, 2484, doi:10.1039/C3PY01630G.
19. Kakuchi, R.; Theato, P., Changing the Reactivity of Polymeric Activated Esters by Temperature: On-Off Switching of the Reactivity of Poly(4-acryloxyphenyldimethylsulfonium triflate). *Macromolecules* **2012,** *45* (3), 1331-1338, doi:10.1021/ma202175z.
20. Kakuchi, R.; Matsubara, K.; Fukasawa, K.; Amii, H., Unveiling α-Etherification Effects on the Aminolysis of α,α-Difluoroacetate Enables the Aminolysis Post-polymerization Modification of α,α-Difluoro-α-(aryloxy)acetate-Containing Polymers. *Macromolecules* **2021,** *54* (13), 6204-6213, doi:10.1021/acs.macromol.1c01027.
21. Kakuchi, R.; Fukasawa, K.; Kikuchi, M.; Narumi, A.; Kawaguchi, S.; Li, Y.; Kim, H.; Amii, H., Computer-Aided Design of Postpolymerization Modification Reaction Based on Aminolysis of α,α-Difluoroacetate Esters. *Macromolecules* **2021,** *54* (1), 364-372, doi:10.1021/acs.macromol.0c02078.
22. Kakuchi, R.; Fukasawa, K.; Chou, L.-C.; Kim, H.; Amii, H., Fundamental insights into aminolysis postpolymerization modification reaction of polymers featuring α,α-Difluoroacetate Esters. *Polymer* **2021,** *230*, 124058, doi:https://doi.org/10.1016/j.polymer.2021.124058.
23. Henkelman, G.; Jónsson, H., Improved Tangent Estimate in the Nudged Elastic Band Method for Finding Minimum Energy Paths and Saddle Points. *J. Chem. Phys.* **2000,** *113* (22), 9978-9985, doi:10.1063/1.1323224.
24. Peng, C.; Bernhard Schlegel, H., Combining Synchronous Transit and Quasi-Newton Methods to Find Transition States. *Isr. J. Chem.* **1993,** *33* (4), 449-454, doi:10.1002/ijch.199300051.
25. Bannwarth, C.; Ehlert, S.; Grimme, S., GFN2-xTB—An Accurate and Broadly Parametrized Self-Consistent Tight-Binding Quantum Chemical Method with Multipole Electrostatics and Density-Dependent Dispersion Contributions. *J. Chem. Theory Comput.* **2019,** *15* (3), 1652-1671, doi:10.1021/acs.jctc.8b01176.
26. Grimme, S.; Bannwarth, C.; Shushkov, P., A Robust and Accurate Tight-Binding Quantum Chemical Method for Structures, Vibrational Frequencies, and Noncovalent

Interactions of Large Molecular Systems Parametrized for All spd-Block Elements (Z = 1–86). *J. Chem. Theory Comput.* **2017,** *13* (5), 1989-2009, doi:10.1021/acs.jctc.7b00118.
27. Bannwarth, C.; Caldeweyher, E.; Ehlert, S.; Hansen, A.; Pracht, P.; Seibert, J.; Spicher, S.; Grimme, S., Extended tight-binding quantum chemistry methods. *WIREs Comput. Mol. Sci.* **2021,** *11* (2), e1493, doi:https://doi.org/10.1002/wcms.1493.
28. Neese, F., Software update: the ORCA program system, version 4.0. *WIREs Comput. Mol. Sci.* **2018,** *8* (1), e1327, doi:https://doi.org/10.1002/wcms.1327.
29. Guo, Y.; Riplinger, C.; Becker, U.; Liakos, D. G.; Minenkov, Y.; Cavallo, L.; Neese, F., Communication: An improved linear scaling perturbative triples correction for the domain based local pair-natural orbital based singles and doubles coupled cluster method [DLPNO-CCSD(T)]. *J. Chem. Phys.* **2018,** *148* (1), 011101, doi:10.1063/1.5011798.
30. Becke, A. D., Density‐Functional Thermochemistry. III. The Role of Exact Exchange. *J. Chem. Phys.* **1993,** *98* (7), 5648-5652, doi:10.1063/1.464913.
31. Lee, C.; Yang, W.; Parr, R. G., Development of the Colle-Salvetti Correlation-Energy Formula into a Functional of the Electron Density. *Phys. Rev. B Condens. Matter* **1988,** *37* (2), 785-789, doi:10.1103/PhysRevB.37.785.
32. Weigend, F.; Ahlrichs, R., Balanced basis sets of split valence, triple zeta valence and quadruple zeta valence quality for H to Rn: Design and assessment of accuracy. *Phys. Chem. Chem. Phys.* **2005,** *7* (18), 3297-305, doi:10.1039/b508541a.
33. Garcia-Ratés, M.; Becker, U.; Neese, F., Implicit solvation in domain based pair natural orbital coupled cluster (DLPNO-CCSD) theory. *J. Comput. Chem.* **2021,** *42* (27), 1959-1973, doi:https://doi.org/10.1002/jcc.26726.
34. Kakuchi, R.; Wongsanoh, K.; Hoven, V. P.; Theato, P., Activation of stable polymeric esters by using organo-activated acyl transfer reactions. *J. Polym. Sci. Part A* **2014,** *52* (9), 1353-1358, doi:https://doi.org/10.1002/pola.27124.
35. Shimomoto, H.; Kudo, T.; Tsunematsu, S.; Itoh, T.; Ihara, E., Fluorinated Poly(substituted methylene)s Prepared by Pd-Initiated Polymerization of Fluorine-Containing Alkyl and Phenyl Diazoacetates: Their Unique Solubility and Postpolymerization Modification. *Macromolecules* **2018,** *51* (2), 328-335, doi:10.1021/acs.macromol.7b01964.
36. Svensson, M.; Humbel, S.; Froese, R. D. J.; Matsubara, T.; Sieber, S.; Morokuma, K., ONIOM: A Multilayered Integrated MO + MM Method for Geometry Optimizations and Single Point Energy Predictions. A Test for Diels−Alder Reactions and Pt(P(t-Bu)3)2 + H2 Oxidative Addition. *J. Phys. Chem.* **1996,** *100* (50), 19357-19363, doi:10.1021/jp962071j.
37. Sure, R.; Grimme, S., Corrected small basis set Hartree-Fock method for large systems. *J. Comput. Chem.* **2013,** *34* (19), 1672-1685, doi:https://doi.org/10.1002/jcc.23317.
38. Grimme, S.; Hansen, A.; Ehlert, S.; Mewes, J.-M.; W., K., r2SCAN-3c: A “Swiss army knife” composite electronic-structure method. *J. Chem. Phys.* **2021,** *154* (6), 064103, doi:10.1063/5.0040021.
39. Spartan 18 or 20, Wavefunction Inc., Irvine CA.
40. Grimme, S., Exploration of Chemical Compound, Conformer, and Reaction Space with Meta-Dynamics Simulations Based on Tight-Binding Quantum Chemical Calculations. *J. Chem. Theory. Comput.* **2019,** *15* (5), 2847-2862, doi:10.1021/acs.jctc.9b00143.
41. Pracht, P.; Bohle, F.; Grimme, S., Automated exploration of the low-energy chemical space with fast quantum chemical methods. *Phys. Chem. Chem. Phys.* **2020,** *22* (14), 7169-7192, doi:10.1039/c9cp06869d.

42. Chemcraft - graphical software for visualization of quantum chemistry computations. https://www.chemcraftprog.com